New Developments in the Regional Atmospheric Modeling System Suitable for Simulations of Snowpack Augmentation over Complex Terrain

Stephen M. Saleeby, William Y. Y. Cheng[1], and William R. Cotton
Department of Atmospheric Science
Campus Delivery 1371
Colorado State University
Fort Collins, CO 80523

Abstract

The Colorado State University Regional Atmospheric Modeling System (RAMS) has been used to emulate cloud seeding operations in the Colorado Rocky Mountains for the winter of 2003-2004 in a previous study (Cotton et al. 2006). This paper documents new developments in RAMS since that study using a winter storm simulation that occurred in Colorado from 3-4 November 2003 as an illustration. The authors reported the advantages and disadvantages in the precipitation prediction of the innermost grid (Δx=3 km) by using the Kain-Fritsch convective parameterization scheme (CPS) in the outer grids in order to reduce the excessive precipitation in the innermost grid. Also, we examined the impacts of the bin-emulation approach to riming on supercooled liquid water prediction and precipitation. The bin-emulation approach alleviated a negative bias in the prediction of cloud liquid water content that occurred in the older microphysics package without this feature. With this new feature, there should be improvements in emulating cloud seeding operations in RAMS.

1. INTRODUCTION

Cotton et al. (2006) described how the Colorado State University Regional Atmospheric Modeling System (RAMS) was used to emulate cloud seeding operations in the Colorado Rocky Mountains during the 2003-2004 winter season as part of the Colorado Weather Damage Modification Program (WDMP). The study uncovered some deficiencies in the model, one of which was the over-prediction of the grid-scale precipitation in the innermost grid (grid 3, Δx=3 km) in a nested grid setup. The over-prediction was more serious for cases in which the flow had a southerly component. Based on past experience with RAMS as a realtime forecast model in Colorado, the authors hypothesized that moist southerly flow contains more moist/unstable air and that the model is unable to resolve the embedded convection within the stratiform clouds, leading to over-prediction of the precipitation in the innermost grid. There was also circumstantial evidence that cloud liquid water content was often under-predicted. This deficiency could result in lower seedabilities than expected in real clouds.

To test these hypotheses, the authors implemented the latest version of the Kain-Fritsch convective parameterization scheme (CPS) (Kain 2004), taken from the Weather Research and Forecasting (WRF) model, in RAMS and activated the Kain-Fritsch CPS in grids 1 (Δx=48 km) and 2 (Δx=12 km) with the concurrent use of the explicit microphysics in all the RAMS grids. The Kain-Fritsch CPS has been widely used in mesoscale simulations, designed for Δx~30 km (e.g., Zhang et al. 2002). The purpose of using the Kain-Fritsch CPS is to parameterize unresolved convection (i.e., dry and stabilize the atmosphere) in the outer grids and letting the drying and stabilizing effect propagate into the innermost grid. As a result, the innermost grid precipitation would be reduced; otherwise, the grid-scale resolved precipitation would be excessive. Previous studies have used the Kain-Fritsch CPS for mesoscale simulations with horizontal grid spacing similar to those of grid 2 (Δx=10-12 km, e.g., Gallus and Segal 2001). However, these studies concentrated mainly on warm season precipitation; the use of CPS in grid spacing of 10-12 km has not been examined for winter season precipitation. Although the fine grid resolved precipitation may be reduced by the use of a CPS in the intermediate nest with grid spacing of 10-12 km, the assumptions of the CPS may be violated. Nonetheless, it is an issue worth examining if the problem of excessive precipitation can be alleviated or reduced. We will document the advantages and disadvantages in the precipitation prediction of the innermost grid by using the Kain-Fritsch CPS in the outer grids. To test the second hypothesis (i.e., the older version of the RAMS microphysics had a negative bias in predicting cloud liquid water content), we will examine the impact of using a refinement in the

[1]Corresponding author address: William Y. Y. Cheng, Department of Atmospheric Science, Campus Delivery 1371, Colorado State University, Fort Collins, Colorado, 80523, Email: cheng@atmos.colostate.edu

microphysics scheme which involved the extension of the bin-emulation approach to include riming processes as described by Saleeby and Cotton (2007).

2. MODEL DESCRIPTION, SETUP, AND INITIALIZATION

2.1 RAMS Description

We used the Colorado State University Regional Atmospheric Modeling System (RAMS@CSU), which is a modified version of RAMS 4.3 (Cotton et al. 2003). This model has been used in a variety of applications such as realtime mesoscale forecasting (Gaudet and Cotton 1998) and simulations of various atmospheric phenomena such as cirrus clouds (Cheng et al. 2001), mesoscale convective systems (Cheng and Cotton 2004), and tornados (Gaudet et al. 2006), as well as regional climate simulations (Saleeby and Cotton 2004a). Some key features of the model include: (i) the interactive Land Ecosystem–Atmosphere Feedback Model, version 2 (LEAF-2; Walko et al. 2000), (ii) an improved two-moment bulk microphysics package (Harrington et al. 1995; Meyers et al. 1997) featuring a large cloud droplet mode (40-80 μm in diameter) and the parameterization of cloud droplet nucleation through the explicit activation of cloud condensation nuclei (CCN) and giant CCN (GCCN) (Saleeby and Cotton 2004b), use of a bin-emulation approach to droplet autoconversion (Tzivion et al. 1987) and the extension of the bin-emulation approach to cloud droplet riming (Saleeby and Cotton 2007), and (iii) a two-stream radiative transfer model coupled to the microphysics package (Harrington et al. 1999). A description of the improved microphysics module follows.

2.2 New Microphysics Module

Briefly, the microphysics of the model is a bulk scheme in which the size-distribution of all hydrometeors is determined by a prescribed generalized gamma distribution. In contrast to most bulk models, however, the physics is explicitly represented by emulating a bin model including the explicit activation of (large and small) cloud droplets and ice particles from CCN and GCCN and ice nuclei (IN), stochastic collection among all hydrometeors using state-of-the-art collection kernels, and a bin representation of sedimentation of hydrometeors. The ice phase is composed of pristine or vapor-grown ice crystals including a variety of habits defined by temperature and saturation conditions, snow which represents partially-rimed vapor-grown ice particles, aggregates, graupel, and hail or frozen raindrops (Meyers et al. 1997; Saleeby and Cotton 2004b).

In a recent cloud-seeding feasibility study with the Colorado Bureau of Reclamation, Cotton et al. (2006) found that realtime RAMS simulations of winter snowfall events, under conditions of moist southwesterly flow, often under-predicted the magnitude and spatial extent of supercooled cloud water and over-predicted total snow water equivalent. It is probable that these two forecasted extrema are related and closely tied to microphysical parameterizations. Given the time-tested robustness of the two-moment cloud nucleation scheme (Saleeby and Cotton 2004b; 2005; Van den Heever et al. 2006; Jiang et al. 2006; Carrió et al. 2006; Comarazamy et al. 2005), it is unlikely that the problem lies with initial cloud formation. Our hypothesis is that cloud water is being depleted by accelerated riming of cloud droplets by ice hydrometeors and/or an overactive Bergeron process due to the coexistence of cloud water and slow falling ice crystals. The efficiency of riming and the parameterized fall speed of ice hydrometeors may strongly impact the cloud water and resultant total precipitation.

Given that the riming process can potentially account for 20% to 50% of snow water equivalent in many mountainous areas of the western United States (Mitchell et al., 1990; Borys et al., 2003), more accurate simulations of this collection process may improve predicted cloud water and snowfall in key areas. The bulk riming scheme in the older RAMS microphysics makes use of a single collection efficiency, determined from the mean mass of the cloud water distribution, to be used to determine the amount of cloud water collected by the various ice species. Use of a single collection efficiency is an imprecise way to determine rimed mass. A binned type riming scheme was, therefore, developed by Saleeby and Cotton (2007) to better compute the amount of rime accreted across the size range of ice and cloud droplet distributions. Individual collection kernels were created for 36 size bins to determine the rimed mass that occurs for all possible particle size interactions between ice species and cloud droplets. The total amount of riming that occurs in a given time step between cloud water and snow, for example, is the sum of the amount of rime that accretes within each bin interaction. It was shown that this binned method *reduces* the degree of total rimed mass and prevents the over-depletion of cloud water. The improved performance of the binned riming scheme over the bulk method becomes especially apparent under heavy riming conditions.

The over-depletion of cloud water may also be impacted by the computation of ice hydrometeor fall speed. If ice particles and cloud droplets co-exist in a grid cell, ambient conditions may often be favorable for the subsequent growth of the ice crystals at the expense of cloud droplets. This would lead to evaporation of supercooled clouds and over-production of ice. The most likely prolonged co-existence of hydrometeors is between cloud droplets and pristine ice crystals due to their very small fall speeds relative to rain, snow, aggregates, graupel, and hail. These two hydrometeor categories are also the most proficient at growth by vapor diffusion; and, by definition, newly formed pristine ice crystals grow solely by vapor diffusion.

RAMS makes use of velocity-diameter power law relations to compute the density-weighted fall speed. These relations are given as $v = c_v D^{p_v}$, where D is diameter, v is fall velocity, and c_v and p_v are the hydrometeor-specific coefficients (Walko et al. 1995; Meyers et al. 1997). A comparative plot of the velocity-diameter power law curves for pristine ice columns is shown in Fig. 1 for the standard RAMS version and the Mitchell (1996) formulation. These fall speed curves suggest that the standard RAMS formula significantly underestimates sedimentation of pristine ice compared to the more recently determined formula. While a higher sedimentation rate of pristine ice would intuitively increase their surface accumulation, it would also reduce growth by the Bergeron process due to shorter residence times at any given level where cloud droplets exist. As a result, we replaced the standard RAMS pristine ice fall speed with the Mitchell (1996) formulation. This would allow more supercooled cloud water to remain, which would enhance potential seedability of such wintertime orographic clouds (Cotton et al. 2006).

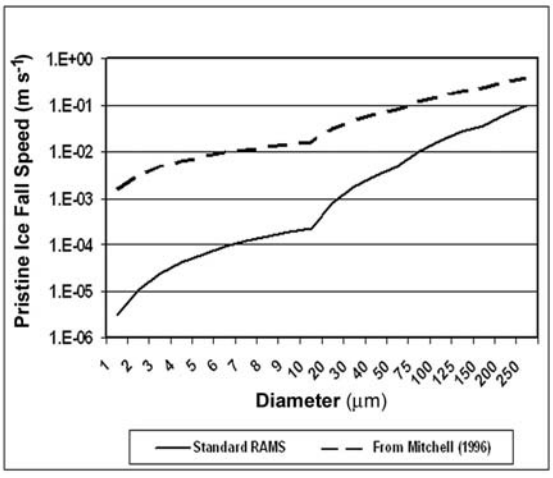

Figure 1. Diameter versus fall speed plots for pristine ice crystals comparing the standard RAMS and Mitchell (1996) power law formulas.

2.3 Kain-Fritsch scheme

The Kain-Fritsch (KF) CPS is a descendant of the Fritsch-Chappel CPS which assumes that the convective effects remove CAPE in a grid volume within an advective time period (Kain and Fritsch 1993). The KF CPS contains three basic components: i) the trigger function, ii) convective updrafts/down-drafts, and iii) the closure assumptions (Kain 2004).

2.3.1 Trigger function

The first order of business for the KF CPS is to identify the so-called "updraft source layers" (USLs) which are potential source layers for convective clouds. The algorithm begins its search at the surface. Vertically adjacent layers in the host model are mixed until the mixture depth is at least 60 hPa, constituting the potential USL. Next, the KF CPS computes the mean thermodynamic properties of this mixture, including the temperature and height of this "parcel" at its lifting condensation level (LCL). Then, the parcel temperature at LCL (T_{LCL}) is compared to that of the environment (T_{ENV}) as a first measure of the likelihood of convective initiation. If this test fails, a temperature perturbation will be added (based on the running-mean vertical velocity and the altitude of the LCL) to the parcel temperature (T_{LCL}) to see whether this temperature exceeds (T_{ENV}). If so, the KF CPS is activated, otherwise, the search is repeated at the next layer and again if necessary until the search goes beyond the lowest 300 hPa of the column.

2.3.2 Convective updrafts/downdrafts

A steady-state entraining-detraining plume model is used to represent convective updrafts in the KF CPS in which equivalent potential temperature (θ_e) and water vapor (q_v) are both entrained and detrained, and various hydrometeors are detrained as well. Evaporation of condensate generated within the updraft generates convective downdrafts. A fraction of this total condensate is allowed to evaporate within the convective downdraft, based on empirical formulas for precipitation efficiency as a function of vertical wind shear and cloud-base height (Zhang and Fritsch 1986). Environmental mass fluxes are required to compensate for the transports in the updrafts and downdrafts in order to keep the net convective mass flux at any level in the column to be zero.

2.3.3 Closure assumptions

The KF CPS removes at least 90% of the convective available potential energy (CAPE) by rearranging the mass in an atmospheric column using the updraft, downdraft, and environmental mass fluxes within an advective time scale (0.5-1 h). CAPE is removed by lowering θ_e in the USL and warming the environment aloft. KF CPS feeds back convective tendencies of temperature, water vapor and cloud water mixing ratios back to the host model.

2.3.4 Improvements in the Kain-Fritsch scheme

Some improvements have been made to the KF CPS since its initial release. The following are some of the highlights.

- The updraft has been modified with a specified minimum entrainment rate to ensure dilution of updraft parcels.
- New formulations in the KF CPS allow for variability in the cloud radius and cloud-depth threshold for deep (precipitating) convection.
- The KF CPS now can account for the effects of non-precipitating shallow convective clouds.

2.4 Use of convective parameterization schemes in RAMS

Until recently, the only CPS available to most of the RAMS community is the Kuo CPS, although other CPSs are available in the non-standard versions (Cotton et al. 2003). However, the Kuo CPS is suitable only for coarse grid spacing, $\Delta x \geq 70$ km (Li et al. 2003). Many users have used the Kuo CPS for $\Delta x \leq 50$ km even though they know that it is not entirely appropriate. For example, Li et al. (2003) used the Kuo CPS in RAMS for a grid of Δx=10 km. Their rationale was that they have no other choice. In our group, most of the research simulations done in RAMS used multiple nested grids with the finest nest down to Δx = 2-3 km and employed only explicit microphysics for all the grids with the coarsest nest at $\Delta x \leq 50$ km (e.g., Bernardet et al. 2000; Nachamkin and Cotton 2000), but our realtime RAMS forecasts have used the Kuo CPS in the coarsest nest (Δx = 48 km) before the KF CPS was available.

When the KF CPS was available for a non-standard version of RAMS, Cheng and Cotton (2004) attempted to use the KF CPS in grids 1 and 2 of a triply nested mesoscale convective system (MCS) simulation (Δx = 50, 12.5, 2.5 km), but decided to neglect CPS in all the grids and used only explicit microphysics (in all grids). They gave the following reasons for this decision:

i. using the KF CPS in grid 2 had negative impact in grid 3, e.g., suppressed and delayed convection.
ii. not using the KF CPS in grid 1 had no large impact in grid 3 (the most important domain).
iii. the KF CPS should be used for horizontal grid spacing of 30 km or less. So, ideally one should not use the KF CPS in grid 1. The other option is to use the Kuo (1974) CPS in grid 1, but the Kuo CPS is more suited to larger grid sizes.
iv. very acceptable cloud-resolving simulations of MCSs on the finest grid using a similar setup as in Cotton and Cheng (2004) have been obtained without convective parameterization.

However, as the use of CPS at Δx = 10-12 km or smaller become more and more widely accepted, we decided to use the KF CPS in grid 2 (Δx = 12 km) to determine if we can remove CAPE on the coarser grids and thereby alleviate the excessive precipitation problem seen in the innermost nest (grid 3) with explicit microphysics (Δx = 2-3 km).

2.5 Model Setup

We used the National Centers for Environmental Prediction (NCEP) Eta analysis to initialize the model atmospheric fields as well as to provide nudging boundary conditions (at six hourly intervals) for grid 1's five outermost grid points. Figure 2 shows the nested grid setup. We used two levels of nesting, with horizontal grid spacing of 48, 12, and 3 km in grids 1, 2, and 3, respectively (Table 1) and 35 terrain-following vertical σ_z levels (Table 2). Note that the grid setup is the same as in Cotton et al. (2006).

Table 1. Nested grid setup.

	number of points in x	number of points in y	horizontal grid spacing (km)
grid 1	100	72	48
grid 2	78	74	12
grid 3	98	98	3

Table 2. Vertical levels (σ_z) used in the simulations (m).

0.0	150.0	300.0	450.0	600.0
750.0	915.0	1 096.5	1 296.2	1 515.8
1 757.3	2 023.1	2 315.4	2 636.9	2 990.6
3 379.7	3 807.6	4 278.4	4 796.2	5 365.9
5 992.5	6 681.7	7 439.9	8 273.9	9 191.3
10 191.3	11 191.3	12 191.3	13 191.3	14 191.3
15 191.3	16 191.3	17 191.3	18 191.3	19 191.3

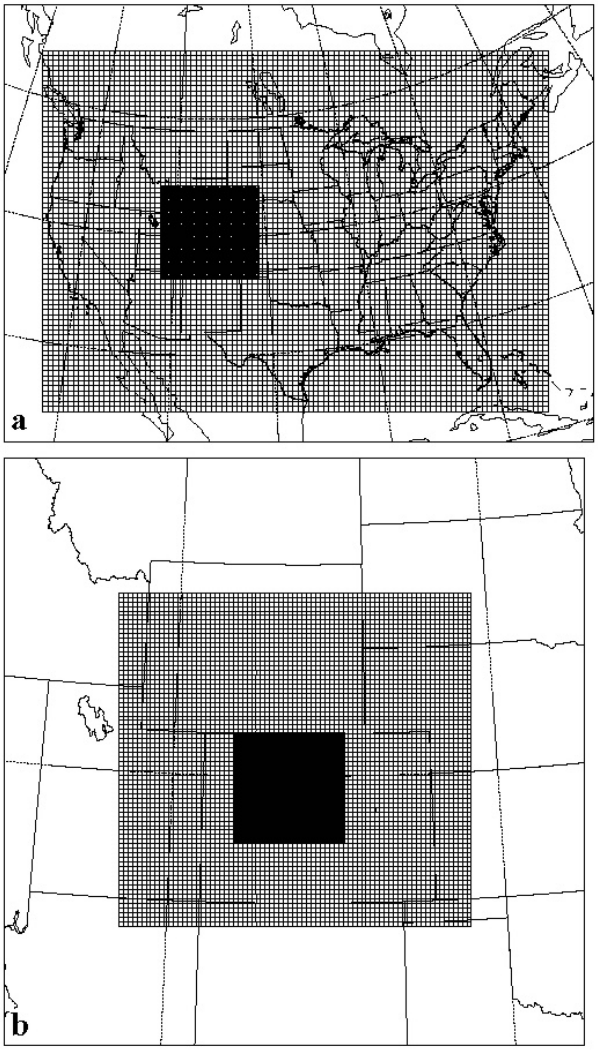

Figure 2. a) Nested grid setup in RAMS with grids 1 and 2; b) nested grid setup in RAMS with grids 2 and 3.

2.6 Experimental Design

The case chosen is the 3-4 November 2003 winter storm from the 2003-2004 WDMP seeding operation over Colorado with south-southwesterly flow in which the grid 3 grid-scale precipitation exceeded SNOTEL by 50% with the older version of RAMS using the Kuo (1974) in grid 1 and a microphysics package without the binned approach to cloud droplet riming (Hartzell et al. 2005). We will focus our results on grid 3 in which the precipitation was explicitly predicted without the use of CPS.

2.6.1 Tests with the Kain-Fritsch convective parameterization

In order to assess the impact of the Kain-Fritsch CPS on the resolved grid 3 precipitation, the authors conducted two experiments. We did not use the Kuo CPS because it is designed mainly for grid sizes much larger than the ones used in this study (discussed in Cheng and Cotton 2004). The experiment in which the Kain-Fritsch CPS was used only in grid 1 was designated as KF1, and the experiment in which the Kain-Fritsch CPS was used in both grids 1 and 2 was designated KF12. For these two experiments, the authors increased the domain of grid 3 from 98 X 98 horizontal grid points to 170 X 170 points to minimize the effects of the Kain-Fritsch CPS in the grid 2/grid 3 interface because the dynamic/thermodynamic effects of the parameterized convection on grids 1 and 2 will be felt by grid 3 on gravity wave timescales through the modification of the grid 3 convective environment by the induced vertical motion (Warner and Hsu 2000). The length of the model integration was for 36 hours. Note that the RAMS microphysics scheme was used in all the grids.

2.6.2 Tests with the new microphysics package

Two comparative simulations were conducted to examine the impact of the new microphysics modification discussed in Section 2.2. The first simulation, hereafter BULKRIME, used the bulk approach to simulate collision/coalescence between ice particles and cloud droplets (riming) and the older fall speed power laws for ice. The second simulation, hereafter BINRIME, used the binned approach to riming (Saleeby and Cotton 2007) and the newly computed fall speed power laws for the ice species (Mitchell 1996). Following the setup discussed in 2.4.1, these simulations employed the Kain-Fritsch CPS on Grids 1 and 2. Furthermore, these model runs used the smaller configuration with 98 X 98 grid points on grid 3. Note that the Kain-Fritsch CPS was used in both grids 1 and 2 in the two simulations.

2.7 Model initialization

At 0000 UTC 3 November 2003 (03/0000 hereafter), the surface analysis featured a continent-wide quasi-stationary front stretching southwestward from the Atlantic coast to the Midwest states and Texas (Fig. 3). From Texas, this quasi-stationary front stretched northwestward to Colorado, Wyoming, and Idaho. The low-level easterly winds in the Front Range of Colorado were the result of a high pressure system

centered over Colorado. Also, the low-level southerly-southwesterly winds in the mountainous regions of central Colorado were caused by a high pressure system with a center over southeastern Texas. At this time, the 650-hPa θ_e map shows the intrusion of high-θ_e air into Colorado from the southwesterly winds. As for the upper-level, the 400-hPa potential vorticity (PV) map featured a high PV strip (*U1*) over the coast of the states of Washington and Oregon and another PV strip (*U2*) over the Pacific and California to Colorado. Southwesterly flow would subsequently advect the PV strip (*U2*) to Colorado around 03/1200. In addition, *U1* would eventually be caught up in the southwesterly flow and be advected over Colorado shortly after 04/0000 (not shown). The upper-level PV strips (*U1* and *U2*) combined with the surface quasi-stationary front and the intrusion of high θ_e into Colorado provided favorable synoptic conditions for the winter storm development from 3-4 November, 2003.

3. RESULTS

3.1 Tests with the Kain-Fritsch Convective Parameterization Scheme

The use of CPSs in mesoscale models is problematic from a conceptual point of view, especially as the horizontal grid spacing decreases, below 10-12 km grid spacing. This is because there is no clear separation between the cloud scale and the mesoscale. Thus, the same physical process may be present in its parameterized and unparameterized forms (Molinari and Dudek 1992). In addition, CPSs are designed to work for certain grid sizes and none of them were designed to work on grid sizes of 10-12 km or smaller. There is no general agreement as to how to handle the use of both explicit microphysics and CPS for grid sizes of 10-12 km or smaller. Nonetheless, for pragmatic reasons, convective parameterizations have been used by a number of researchers for grid sizes of 10-12 km or smaller to reduce excessive grid-scale precipitation (e.g., Gallus and Segal 2001).

Figure 4 shows the (liquid equivalent) accumulated precipitation in grid 3 from 03/0800 to 04/0800, and Fig. 5 displays the primary mountain ranges in grid 3. Both KF1 and KF2's precipitation accumulations show high spatial correlation with the terrain, such as the precipitation maxima over the Flat Tops, Sawatch Range, and Gore Range. However, with the activation of the Kain-Fritsch CPS in grid 2, KF12 reduced not only the amplitude of the precipitation maxima by more than a factor of 2 as compared to KF1, but the accumulated precipitation was less widespread in

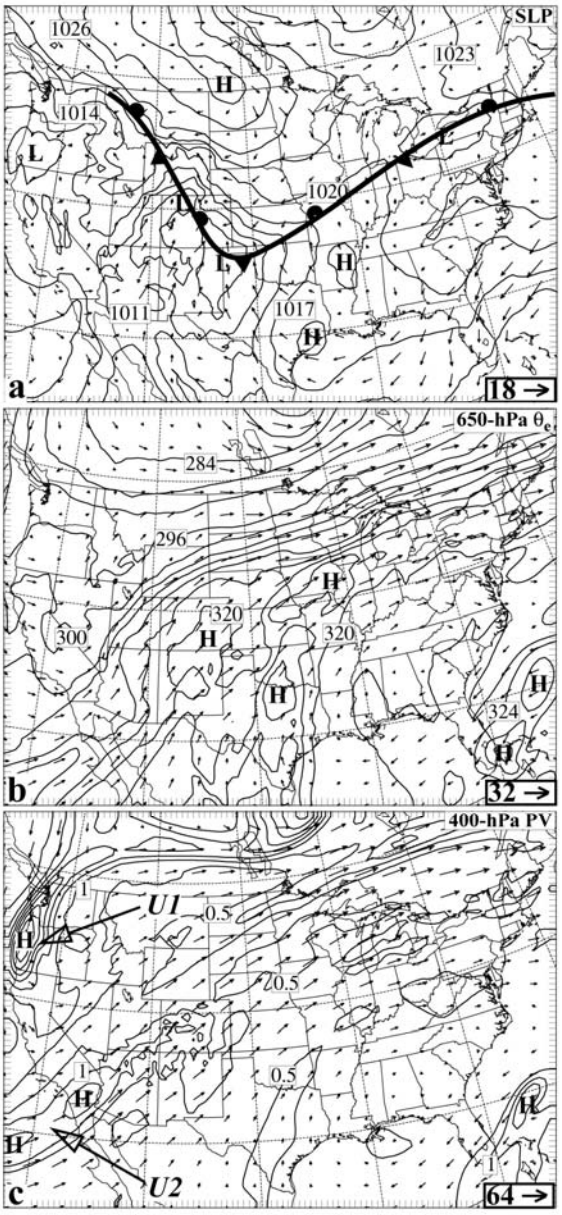

Figure 3. Model initial conditions in grid 1 interpolated from Eta analysis at 03/0000: a) sea-level pressure (contour intervals of 3 hPa) superposed with wind vectors at the lowest σ_z level; b) 650-hPa equivalent potential temperature (contour intervals of 4 K) superposed with 650-hPa wind vectors; c) 400-hPa potential vorticity (with contour intervals of 0.5 PVU) superposed with 400-hPa wind vectors. Insets represent the scale of the wind vectors in m s^{-1}.

KF12. For example, two of the 24-h accumulated precipitation maxima over the Gore Range in KF1 reduced from >40 to 20 mm and from 60 to 30 mm,

respectively, in KF12. Similarly, the precipitation maxima in the Sawatch Range was >60 mm in KF1 and was reduced >20 mm in KF12. In Fig. 6, the (liquid equivalent) maximum three-hourly precipitation accumulation time series[1] also demonstrates similar results, with KF12 reducing the maximum three-hourly precipitation accumulation by a factor of 2 or more after 03/1200. These results can be explained by the fact that activating the Kain-Fritsch CPS in grid 2 caused the atmosphere to be drier and more stable. Thus, the atmospheric boundary conditions provided by grid 2 to grid 3 were also drier and more stable. The domain-averaged precipitable water was also reduced in KF12 by at least 1-2 mm for most forecast hours (Fig. 7).

For the available 61 SNOTEL stations over grid 3, the average snow water equivalent for the 24-h accumulation ending at 04/0800 was 10 mm, as shown in Fig. 8. The corresponding value for KF1 (KF12) was just above 12 mm (about 2.5 mm). These results are also consistent with the 700-500-hPa relative humidity showing KF12 to be substantially drier than KF1 (not shown).

3.2 Tests with the New Microphysics Package

With the use of the improved microphysics in RAMS, it is suspected that the cloud water field will be impacted by both the state of the art binned riming method and improved ice fall speeds equations. This impact could strongly influence seedability in such future simulations and overcome previous model seeding difficulties.

Since our initial primary concern was the over-prediction of precipitation, we will examine the differences in total liquid equivalent precipitation between the BULKRIME and BINRIME simulations. Figure 9 displays the negative and positive precipitation changes at 36 hours into the simulations. There was no consistent domain-wide response to accumulation with the use of the BINRIME microphysics scheme. However, over the western portion of the domain, there was a trend whereby increases in precipitation were found upwind and downwind of peaks in the highest terrain, while decreases were found right along the highest mountain ridges. These precipitation differences were very likely due to reduced riming within orographic clouds along high mountain ranges as well as the modified fall speeds. Reduced riming produced smaller snow crystals and greater amounts of snow "blowover" to the leeward slopes of mountain ranges (Hindman 1986; Saleeby et al. 2006). This would tend to shift the ridgetop snow downstream. The precipitation increase on the windward slopes may be solely due to greater ice crystal fall speed, but this is difficult to determine without a specific microphysical process study along the affected mountain ranges.

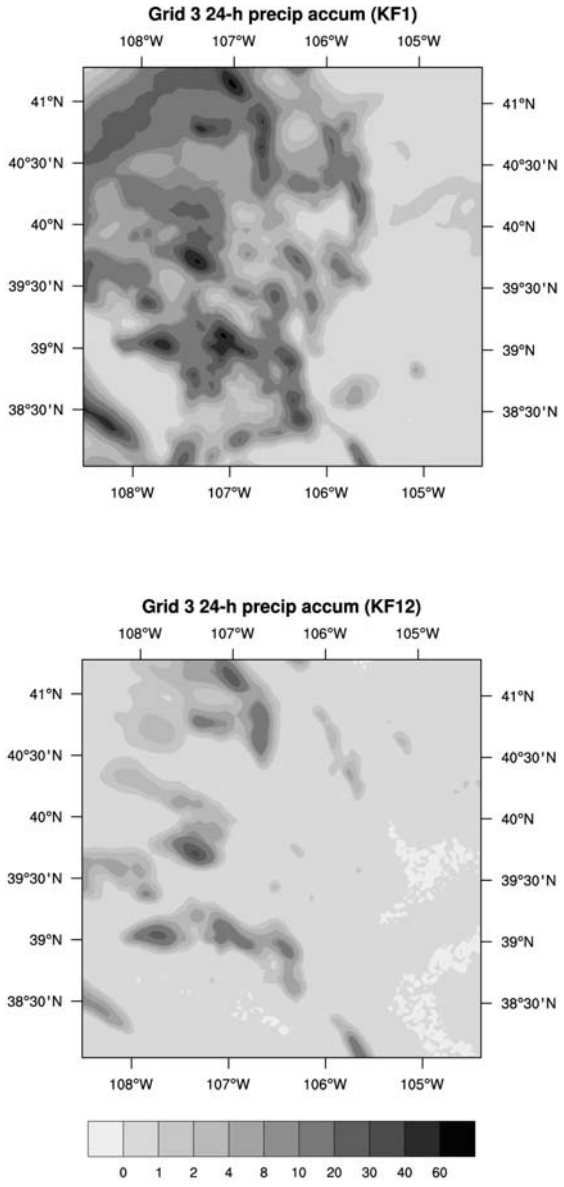

Figure 4. 24-h (liquid equivalent) precipitation accumulation (mm) from 03/0800 to 04/0800 in grid 3 for KF1 (top panel); b) KF12 (bottom panel).

[1] Note that for experiments KF1 and KF2 in which an expanded domain was used, the maximum precipitation accumulation and the domain average in grid 3 excluded the 25 outermost grid points in order to avoid the problems of spurious precipitation at the grid 2/grid 3 interface. This problem of spurious precipitation was likely the result of the interaction of the complex terrain and the propagation of the effects of the parameterized convection from grid 2 to grid 3.

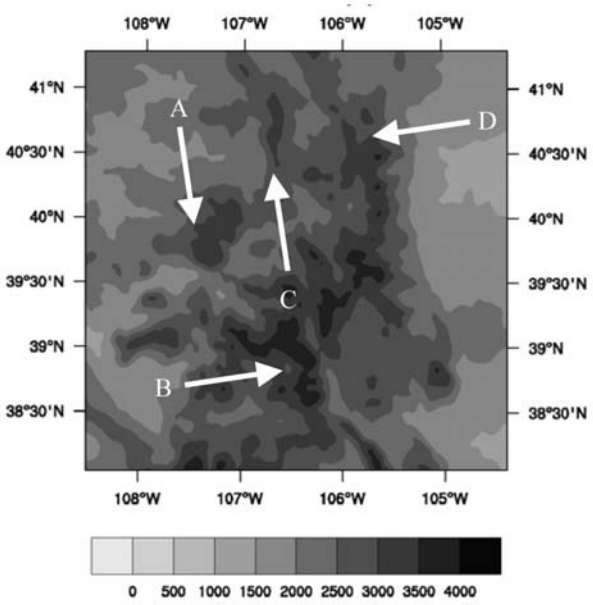

Figure 5. Expanded grid 3 terrain (m). Note that the 25 outermost grid points are not shown. A: Flat Tops; B: Sawatch Range; C: Gore Range; D: Medicine Bow Mountains.

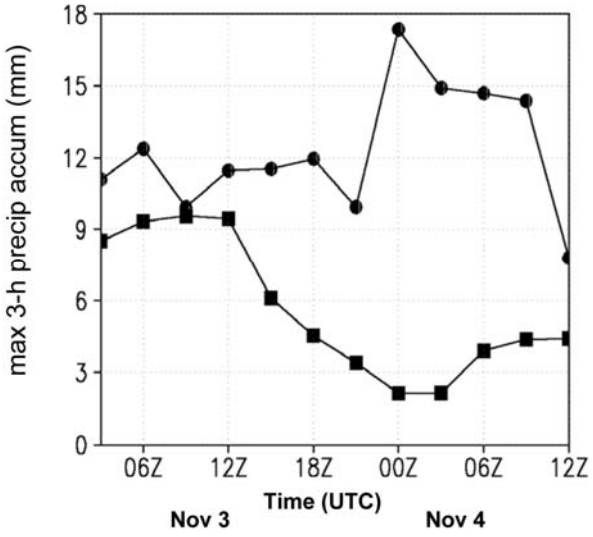

Figure 6. Expanded grid 3 (liquid equivalent) maximum three-hourly precipitation accumulation (mm) for KF1 (circle) and KF12 (square). Note that the 25 outermost grid points were not considered.

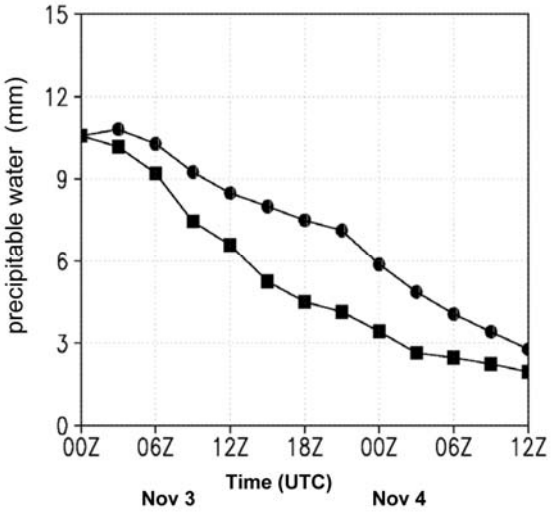

Figure 7. Expanded grid 3 domain-averaged precipitable water (mm) for KF1 (circle) and KF12 (square). Note that the 25 outermost grid points were not considered.

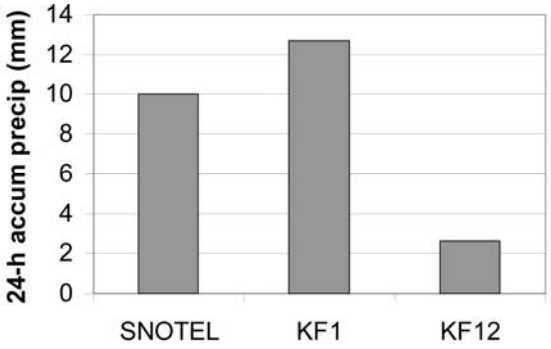

Figure 8. Average of 24-h (liquid equivalent) precipitation accumulation (mm) from 03/0800 to 04/0800 for 61 selected stations in Colorado for SNOTEL, KF1 (grid 3), and KF2 (grid 3).

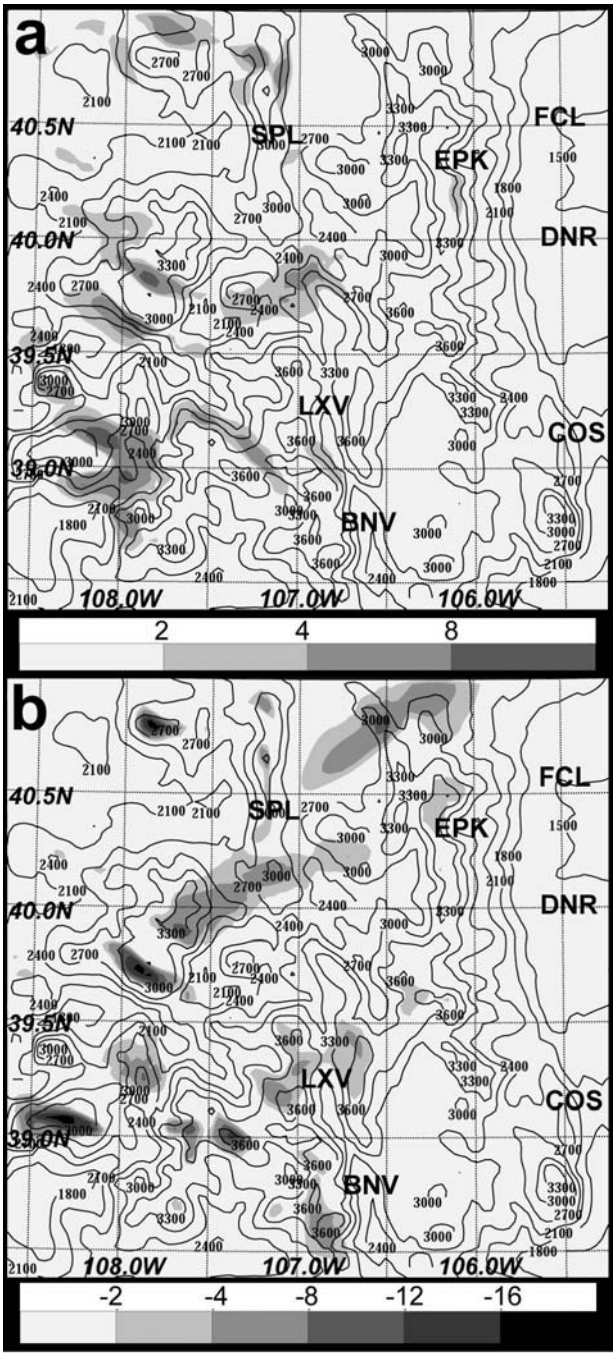

Figure 9. Total precipitation difference (mm) on grid-3 between the simulation using the new ice fall speeds and binned riming and the simulation with old ice fall speeds and bulk riming (BINRIME - BULKRIME). Panels display areas of precipitation that experience an (a) increase and (b) decrease. Topography (m) is contoured. The following locations are given for reference: FCL-Fort Collins, DNR-Denver, COS-Colorado Springs, SPL-Storm Peak Lab, LXV-Leadville, and BNV-Buena Vista.

The cloud water field responded to the BINRIME parameterizations as in our hypothesis, with significant increases across the affected portions of the domain. The vertically- integrated cloud water difference field is shown in Fig. 10 at the time of its magnitude maximum. At the particular time shown, there was a large areal increase in cloud water over the northwest portion of the domain, with maximum differences over the peaks in the topography. There were several other more localized areas of increased cloud water, over the west-central portion of the domain, associated with orographic maxima. These patterns suggest that the BINRIME microphysics imposes its greatest magnitude impact on orographic clouds, where the seeder-feeder process is often very active. As an example of this impact, Fig. 11 displays a west-to-east cross-section centered on the grid row closest to Storm Peak Lab in the Park Range of CO (40.45N, 106.73W). This area is known for its frequent orographic cloud production during winter months (Borys et al. 2003; Saleeby and Cotton 2005). This cross-section reveals several key differences between the BULKRIME and BINRIME simulations. Primarily, the orographic cloud was of greater expanse due to reduced depletion by riming by the binned riming scheme. The reduction in riming also directly led to a reduction in snow and aggregate mixing ratio. Furthermore, a reduction in riming means that less wet growth will occur. Since wet growth is required for production of graupel, there is very little graupel present with use of the BINRIME microphysics parameterizations.

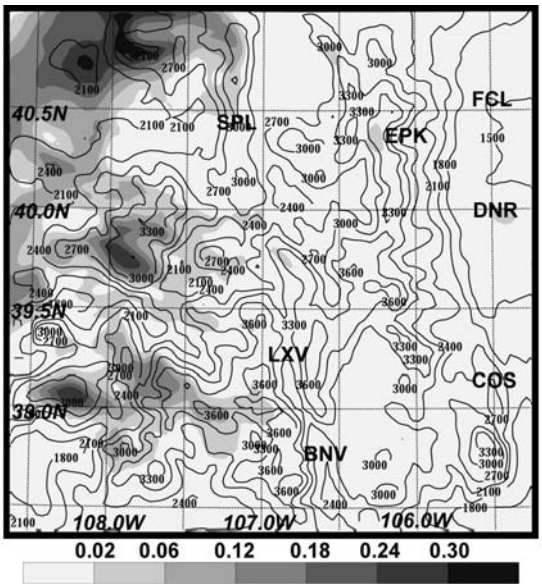

Figure 10. Vertically integrated cloud water difference (mm) on grid-3 between the simulation using the new ice fall speeds and binned riming and the simulation with old ice fall speeds and bulk riming, (BINRIME - BULKRIME), at the time of maximum cloud water. Topography (m) is contoured.

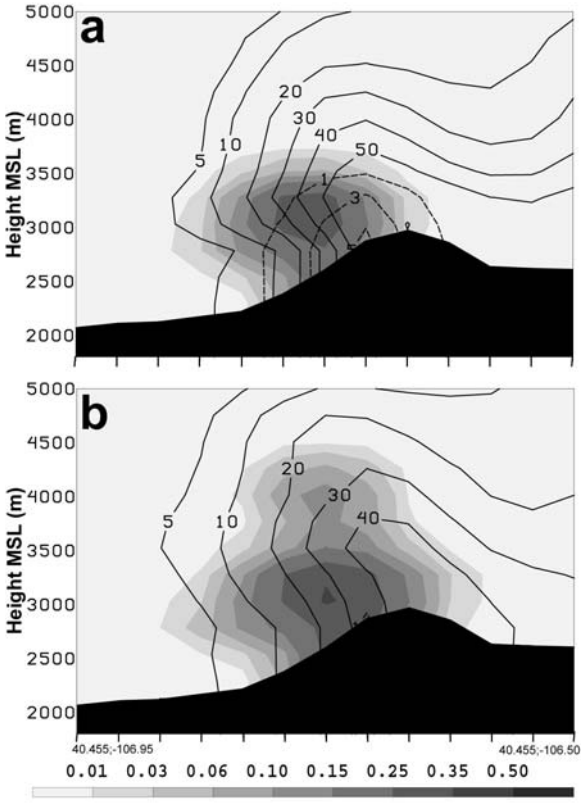

Figure 11. West to east vertical cross-section through the Park Range on Grid-3 nearest to Mt. Werner. Plots display cloud water mixing ratio (g kg^{-1}, shaded), snow+aggregates (g kg^{-1} x 100, solid contours), and graupel (g kg^{-1} x 100, dashed contours). Panel (a) plotted from simulations using the old ice fall speeds and bulk riming, and panel (b) plotted from simulations using the new ice fall speeds and binned riming. Cross-section was taken at the time of maximum cloud water along the Park Range (04 Nov 0600 UTC).

Examination of domain-wide bulk quantities provides further insight into the impacts of the microphysics modifications in this study. Figure 12 displays time series of several vertically-integrated, domain-summed cloud processes for the BULKRIME and BINRIME simulations. The times series comparing the cloud water mixing ratio shows that the total cloud water in the BINRIME simulation is greater at all times, with the greatest increase at the time of the domain maximum during this event. The plot of rimed cloud water exhibits a decrease in the BINRIME simulations at all times throughout the simulation. The reduced riming was a dominant reason why a greater amount of cloud water was retained when using the binned riming method. The other primary reason for greater liquid water was the reduced vapor growth of

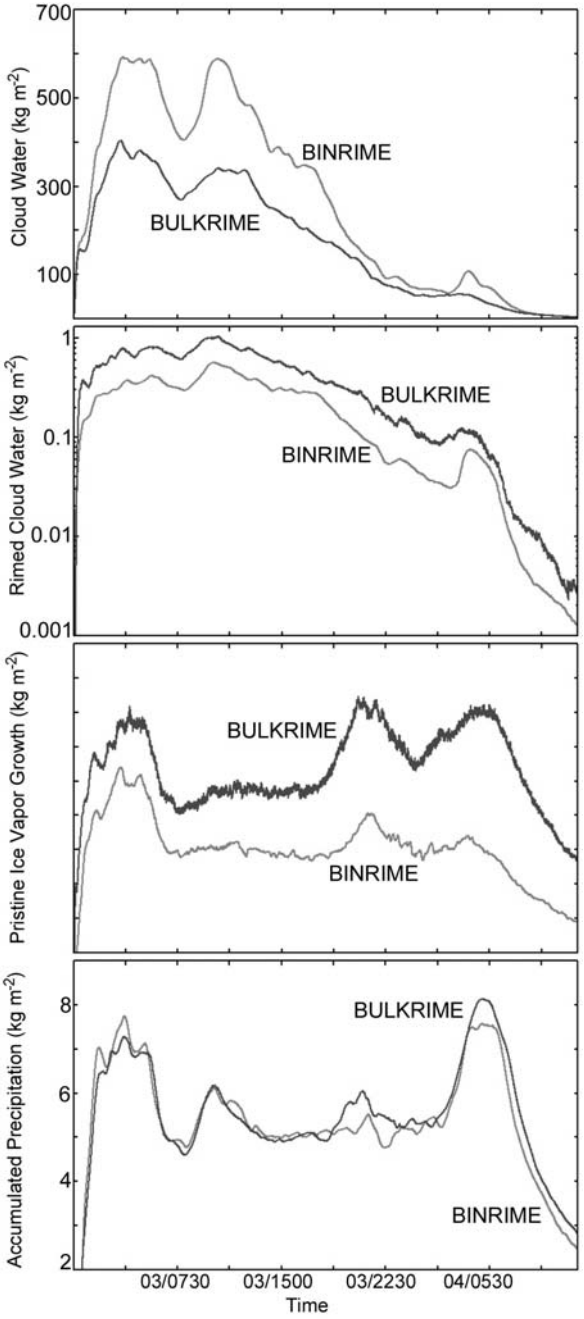

Figure 12. Time series of domain-summed quantities comparing use of the old fall speed power laws and bulk riming (BULK) with the new fall speed power laws and binned riming (BINRIME) in grid 3. Panel (a) displays cloud water, (b) amount of rime, (c) vapor growth of pristine ice, and (d) accumulation of precipitation. Units of (kg m^{-2}) denote vertically integrated quantities. Multiplying by area of the domain gives mass totals.

pristine ice, which often occurs at the expense of cloud droplet evaporation in ice-saturated and water-subsaturated environments. The time series of pristine ice vapor growth reveals a consistent reduction of vapor depositional growth as a result of the increased pristine ice fall speeds. The greater fall speed reduced the overall atmospheric residence time for ice particles undergoing vapor deposition whether in-cloud or out-of-cloud. Though not shown, the vapor growth of cloud droplets responded with a time-averaged increase of nearly 20%. This model response emphasizes the importance of representing hydrometeor fall speeds as precisely as possible. The last plot displays the time series of surface precipitation for the duration of the event. The precipitation variability between the two simulations does not produce a clear increasing or decreasing trend that favors either simulation. Towards the end of the model runs, the BINRIME simulation produced less precipitation, but this difference is of little consequence. The total precipitation can be influenced by model dynamics and parameterized convection in the outer grids, thus potentially masking any dominant microphysical trend that may exist. Regardless, the overall difference in accumulated precipitation produced a decrease of 2% in the BINRIME simulation when compared to BULKRIME.

4. DISCUSSION AND SUMMARY REMARKS

We have evaluated the impact of using the Kain-Fritsch CPS in grid 2 in grid 3 of the RAMS simulation. Specifically, using the Kain-Fritsch CPS in grid 1 only resulted in unrealistically (large) precipitation maxima in grid 3. Using the Kain-Fritsch CPS in both grids 1 and 2 had the desired effect of reducing the amplitude of the precipitation maxima in grid 3. However, the spatial coverage of the precipitation was suppressed as well. This is consistent with the results reported in Cheng and Cotton (2004) in which convection was suppressed and delayed in the innermost grid (3) with $\Delta x = 2.5$ km with the KF CPS activated in grids 1 and 2 in a MCS simulation. It is computationally expensive not to employ a nested grid setup for the simulations such as the one in this study. Thus, the researcher has to decide whether or not a CPS should be employed in grid spacing such as in grid 2 where the use of a CPS is problematic. Kain and Fritsch (1998) argued that CPS may be necessary even at horizontal grid spacing of 5 km. Gallus and Segal (2001) simulated 20 cases of MCSs with various combinations of different CPSs and model initial conditions using the workstation Eta Model at a horizontal grid spacing of 10 km. Although some cases performed better without CPS, Gallus and Segal found that the model skill scores were higher when they employed a CPS in their simulations. However, for an extensive case study, Warner and Hsu (2000) found that convective parameterization in the coarser grids have negative impacts in the inner grids. It is well known that explicit simulations (without the use of CPSs) tend to produce excessive precipitation even at horizontal grid spacing of 4 km in other models such as WRF (Weisman et al. 2005). The difficult question to answer is, which approach is better? Clearly, without the CPS in grid 2, the grid 3 resolved precipitation maxima was too large. However, with the CPS activated in grid 2, the grid 3 resolved precipitation maxima were reduced to the detriment of suppressing the overall precipitation in grid 3. Perhaps there can be a solution. Ensemble forecasting is getting more and more acceptance in numerical weather prediction. Perhaps the same approach can be applied here. The user can take an ensemble average of the two simulations.

A boundary layer cloud parameterization using double Gaussian probability density functions (PDFs) with a higher-order closure has been developed in the Cotton group (Golaz et al. 2002). This boundary layer cloud parameterization can handle shallow embedded convection. The use of this boundary layer cloud parameterization in mesoscale models for shallow embedded convection such as in this southerly flow case is more appropriate than using CPSs designed specifically for deep convection (e.g., Kain-Fritsch CPS). However, it may be some years away before we can see this boundary layer cloud parameterization operational in mesoscale models such as RAMS.

The microphysical modifications, including the binned riming scheme and the newly adapted power laws for ice hydrometeor fall speed, provide a more realistic representation of the riming and sedimentation processes, respectively. These adaptations arise from more modern laboratory and mathematical studies used to more accurately quantify these microphysical processes. As mentioned previously, the overall accumulated precipitation across the domain was only slightly modified. However, the amount of riming was reduced, the Bergeron process was reduced, vapor growth of cloud water was increased, and the domain cloud water field was increased. The results suggest that the limited seeding impact seen in Cotton et al. (2006) may have been the result of poorly represented riming and poorly estimated ice hydrometeor fall speeds. Future model seeding studies would be needed to confirm this hypothesis. It should also be noted again that the BINRIME and BULKRIME simulations used the KF parameterization on both grids 1 and 2.

From the results discussed above, the use of the cumulus scheme on grid 2 may have suppressed the microphysics on grid 3 in both simulations. As such, it is likely that the impacts of the binned riming and newer fall speeds would be greatly accentuated had the microphysics and precipitation processes been more active with KF on grid 1 only.

5. ACKNOWLEDGEMENTS

This work was supported by grants provided by Center for Geosciences/Atmospheric Research (contract # W911NF-06-2-0015) and the National Science Foundation (contract #ATM-0451439). The authors appreciate comments from the editor, Dr. Andrew Detwiler, and an anonymous reviewer.

6. REFERENCES

Bernardet, L. R. , L. D. Grasso, J. E. Nachamkin, C. A. Finley, and W. R. Cotton, 2000: Simulating convective events using a high-resolution mesoscale model. *J. Geophys. Res.*, **105**, 14 963–14 982.

Borys, R. D., D. H. Lowenthal, S. A. Cohn, and W. O. J. Brown, 2003: Mountaintop and radar measurements of anthropogenic aerosol effects on snow growth and snowfall rate. *Geo. Res. Lett.*, **30**, 1538, doi:10.1029/2002GL016855.

Carrió, G. G., S. C. van den Heever, and W. R. Cotton, 2006: Impacts of nucleating aerosol on anvil-cirrus clouds: A modeling study. *Atmos. Res.*, In press.

Cheng , W. Y. Y., T. Wu, and W. R. Cotton, 2001: Large-eddy simulations of the 26 November 1991 FIRE II cirrus case. *J. Atmos. Sci.*, **58**, 1017-1034.

_____, and W. R. Cotton, 2004: Sensitivity of a cloud-resolving simulation of the genesis of a mesoscale convective system to horizontal heterogeneities in soil moisture initialization. *J. Hydromet.*, **5**, 934-958.

Comarazamy, D. E., J. E. Gonzalez, C. A. Tepley, S. Raizada, and R. V. R. Pandya, 2006: Effects of atmospheric particle concentration on cloud microphysics over Arecibo. *J. Geophys. Res.*, **111**, 9205, doi:10.1029/2005JD006243.

Cotton, W.R., and Co-authors, 2003: RAMS 2001: Current status and future directions. *Meteorol. Atmos. Phys*., **82**, 5-29.

_____, R. McAnelly, G. Carrió, P. Mielke, and C. Hartzell, 2006: Simulations of snowpack augmentation in the Colorado Rocky Mountains. *J. Wea. Mod.*, **38**, 58-65.

Gallus, W. A., and M. Segal, 2001: Impact of improved initialization of mesoscale features on convective system rainfall in 10-km Eta simulations. *Wea. Forecasting*, **16**, 680–696.

Gaudet, B. J., and W. R. Cotton, 1998: Statistical characteristics of a realtime precipitation forecasting model. *Wea. Forecasting*, **13**, 966-982.

_____, and _____, 2006: Low-level mesocyclonic concentration by non-axisymmetric processes. Part I: Supercell and mesocyclone evolution. *J. Atmos. Sci.*, **63**, 1113-1133.

Golaz, J.-C., V. E. Larson, and W. R. Cotton, 2002: A PDF-based model for boundary layer clouds. Part I: Method and model description. *J. Atmos. Sci.*, **59**, 3540–3551.

Harrington, J. Y., M. P. Meyers, R. L. Walko, and W. R. Cotton, 1995: Parameterization of ice crystal conversion processes due to vapor deposition for mesoscale models using double-moment basis functions. *J. Atmos. Sci.*, **52**, 4344–4366.

_____, T. Reisin, W. R. Cotton, and S. M. Kreidenweis, 1999: Cloud resolving simulations of Arctic stratus. Part II: Transition-season clouds. *Atmos. Res.*, **51**, 45–75.

Hartzell, C., W. Cotton, R. McAnelly, G. Carrio. P. Mielke, J. Busto, S. Schmitzer, L. Hjermstad, R. Williams, 2005: Numerical Simulations of Snowpack Augmentation for Drought Mitigation Studies in the Colorado Rocky Mountains. Final Report (available from the CWCB) and at http://rams.atmos.colostate.edu/clseeding/prog-reports.html

Hindman, E. E., 1986: Characteristics of supercooled liquid water in clouds at mountaintops in the Colorado Rockies. *J. Clim. Appl. Meteor.*, **25**, 1271-1279.

Jiang, H., and W. R. Cotton, 2005: A diagnostic study of subgrid-scale activation. *J. Geophys Res.*, **110**, D16107, doi:1029/2004JD005722.

Kain, J. S., and J. M. Fritsch, 1998: Multiscale convective overturning in mesoscale convective systems: Reconciling observations, simulations, and theory. *Mon. Wea. Rev.*, **126**, 2254-2273.

_____, 2004: The Kain–Fritsch convective parameterization: An update. *J. Appl. Met.*, **43(1)**, 170-181.

Kuo, S. L., 1974: Further studies of the parameterization of the effect of cumulus convection on large-scale flow. *J. Atmos. Sci.*, **31**, 1232–1240.

Meyers, M. P., R. L. Walko, J. Y. Harrington, and W. R. Cotton, 1997: New RAMS cloud microphysics parameterization. Part II: The two-moment scheme. *Atmos. Res.*, **45**, 3–39.

Mitchell, D. L., R. Zhang., and R. L. Pitter, 1990: Mass dimensional relationships for ice particles and the influence of riming on snowfall rates. *J. Appl. Meteor.*, **29**, 153-163.

_____, 1996: Use of mass- and area-dimensional power laws for determining precipitation particle terminal velocities. *J. Atmos. Sci*., **53**, 1710-1723.

Molinari, J., and M. Dudek, 1992: Parameterization of convective precipitation in mesoscale numerical models: A critical review. *Mon. Wea. Rev.*, **120**, 326-344.

_____, and _____, 1994: Reply to Comments on "Parameterization of convective precipitation in mesoscale numerical models: A critical review". *Mon. Wea. Rev.*, **122**, 2232-2233.

Nachamkin, J. E., and W. R. Cotton, 2000: Interactions between a developing mesoscale convective system and its environment. Part II: Numerical simulation. *Mon. Wea. Rev.*, **128**, 1225–1244.

Saleeby, S. M., and W. R. Cotton, 2004a: Simulations of the North American monsoon system. Part I: Model analysis of the 1993 monsoon season. *J. Climate*, **17**, 1997-2018.

_____, and _____, 2004b: A large droplet mode and prognostic number concentration of cloud droplets in the Colorado State University Regional Atmospheric Modeling System (RAMS). Part I: Module descriptions and supercell test simulations. *J. Appl. Meteor.*, **43**, 182-195.

_____, and _____, 2005: A large-droplet mode and prognostic number concentration of cloud droplets in the Colorado State University Regional Atmospheric Modeling System (RAMS). Part II: Sensitivity to a Colorado winter snowfall event. *J. Appl. Meteor.,* **44**, 1912-1929

_____, and _____, 2007: A binned approach to cloud droplet riming implemented in a bulk microphysics model. *J. Appl. Met.*, Submitted.

_____, R. D. Borys, M. A. Wetzel, D. Simeral, M. P. Meyers, W. R. Cotton, R. McAnelly, N. Larson, E. Heffernan, 2006: Model aerosol sensitivity studies and microphysical interactions in an orographic snowfall event. *12th AMS Conference on Mountain Meteorology*, 6pp.

Tzivion, S., G. Feingold, and Z. Levin, 1987: An efficient numerical solution to the stochastic collection equation. *J. Atmos. Sci.*, **44**, 3139-3149.

Van den Heever, S. C., G. G. Carrió, W. R. Cotton, P. J. DeMott, and A. J. Prenni, 2006: Impacts of nucleating aerosol on Florida convection. Part I: Mesoscale simulations. *J. Atmos. Sci.*, **63**, 1752-1775.

Walko, R. L., W. R. Cotton, M. P. Meyers, and J. Y. Harrington, 1995: New RAMS cloud microphysics parameterization: Part I. The single-moment scheme. *Atmos. Res*., **38**, 29-62.

_____, and Co-authors, 2000: Coupled atmosphere–biophysics–hydrology models for environmental modeling. *J. Appl. Meteor.*, **39**, 931–944.

Warner, T. T., and H. M. Hsu, 2000: Nested-model simulation of moist convection: The impact of coarse-grid parameterized convection on fine-grid resolved convection. *Mon. Wea. Rev.*, **128**, 2211–2231.

Weisman, M., W. Wang, and C. Davis, 2005, Experiences with 0-36 hour explicit convective forecasting with the WRF-ARW model. 6th WRF / 15th MM5 Users' Workshop, Boulder , CO.

Zhang D.-L., and J. M. Fritsch, 1986: Numerical simulation of the meso-β scale structure and evolution of the 1977 Johnstown flood. Part I: Model description and verification. *J. Atmos. Sci.*, **43**, 1913–1943.

_____, W. Y. Y. Cheng, and J. R. Gyakum, 2002: The impact of various potential vorticity anomalies on multiple frontal cyclogenesis events. *Q. J. R. Meteorol. Soc.*, **128**, 1847-1878.